Biomarker Analysis and Treatment Dynamics Following Preoperative Ipilimumab plus Nivolumab in Locally Advanced Urothelial Cancer from the Phase IB NABUCCO Study

Chantal F. Stockem[1], Alberto Gil-Jimenez[2], Hamza Ali[2], Jeroen van Dorp[2], Nick van Dijk[1], Maurits L. van Montfoort[3], Maartje Alkemade[4], Annegien Broeks[4], Iris M. Seignette[3], Erik Hooijberg[3], Wim Brugman[5], Rhianne Voogd[6], Bas W.G. van Rhijn[7,8], Laura S. Mertens[7], Jeantine M. de Feijter[1], Niven Mehra[9], Antoine G. van der Heijden[10], Richard P. Meijer[11], Britt B.M. Suelmann[12], Wouter Scheper[6], Lodewyk F.A. Wessels[2,13,14], Daniel J. Vis[2,13], and Michiel S. van der Heijden[1,2]

ABSTRACT

Purpose: In NABUCCO, the safety and efficacy of preoperative ipilimumab plus nivolumab were assessed in stage III urothelial cancer. Encouraging responses were achieved, and ipilimumab 3 mg/kg (ipilimumab-high) seemed more effective than ipilimumab 1 mg/kg (ipilimumab-low). We explored ipilimumab plus nivolumab response biomarkers and tumor microenvironment (TME) treatment dynamics.

Patients and Methods: Baseline formalin-fixed, paraffin-embedded tumor tissue was analyzed using PD-L1 IHC ($n = 51$) and whole-exome and transcriptome sequencing (both $n = 53$) and correlated with response. Baseline infiltration of $CD8^+$ T cells ($n = 51$) and at cystectomy ($n = 42$) was examined. Single-cell RNA sequencing (scRNA-seq) of $CD3^+$ T cells was conducted on on-treatment resection tissue of two responders to ipilimumab-high to explore the characteristics of $CD8^+$ T cells within the TME.

Results: High tumor mutational burden and PD-L1 positivity were associated with response to ipilimumab plus nivolumab. Nonresponding patients exhibited increased expression of a TGFβ signature. We observed increased transcription of the g2m checkpoint and e2f target in responders to ipilimumab-high and enhanced transcription of IFN-α and IFN-γ hallmarks in responders to ipilimumab-low. $CD8^+TCF7^+$ T cells accumulated in the TME of responders to ipilimumab-high. scRNA-seq of *CD8A*$^+$*TCF7*$^+$ T cells demonstrated enhanced expression of *IL7R*, *CCR7*, *GPR15*, *XCL1*, *SELL*, and *LEF1*.

Conclusions: Our data indicate that tumor mutational burden, PD-L1, and TGFβ are potential biomarkers for response to ipilimumab plus nivolumab in stage III urothelial cancer. An inflammatory TME might be relevant for responding to ipilimumab-low. We found that in responders to ipilimumab-high, $TCF7^+CD8^+$ T cells accumulated in the TME. scRNA-seq in two responders suggested that *TCF7*$^+$*CD8A*$^+$ T cells express genes associated with immunologic memory formation and T-cell homing.

Introduction

The standard surgical treatment for nonmetastatic muscle-invasive bladder cancer is radical cystectomy and pelvic lymph node dissection, ideally preceded by cisplatin-based neoadjuvant chemotherapy. However, the benefit of neoadjuvant chemotherapy is modest (1). Despite curative intent, recurrence rates are substantial, especially in patients with locoregionally advanced stage III urothelial cancer (cT3-4aN0M0 or cT1-4aN1-3M0).

Therapies targeting inhibitory immune checkpoints, such as PD-(L)1 and CTLA-4, have been explored for over a decade. The initial trials evaluated anti–PD-(L)1 monotherapy in metastatic urothelial cancer (2–4) and demonstrated that durable responses could be achieved in a subset of patients. Based on data indicating that immune checkpoint blockade (ICB) may be even more potent when administered preoperatively (5), PD-(L)1 blockade has also been applied in the preoperative setting in combination with neoadjuvant chemotherapy (6) or as monotherapy (7, 8). Even though response

[1]Department of Medical Oncology, Netherlands Cancer Institute, Amsterdam, the Netherlands. [2]Department of Molecular Carcinogenesis, Netherlands Cancer Institute, Amsterdam, the Netherlands. [3]Department of Pathology, Netherlands Cancer Institute, Amsterdam, the Netherlands. [4]Core Facility Molecular Pathology & Biobanking, Netherlands Cancer Institute, Amsterdam, the Netherlands. [5]Genomics Core Facility, Netherlands Cancer Institute, Amsterdam, the Netherlands. [6]Department of Molecular Oncology and Immunology, Netherlands Cancer Institute, Amsterdam, the Netherlands. [7]Department of Surgical Oncology (Urology), Netherlands Cancer Institute, Amsterdam, the Netherlands. [8]Department of Urology, Caritas St. Josef Medical Centre, University of Regensburg, Regensburg, Germany. [9]Department of Medical Oncology, Radboud University Medical Center, Nijmegen, the Netherlands. [10]Department of Urology, Radboud University Medical Center, Nijmegen, the Netherlands. [11]Department of Oncological Urology, University Medical Center Utrecht, Utrecht, the Netherlands. [12]Department of Medical Oncology, University Medical Center Utrecht, Utrecht, the Netherlands. [13]Oncode Institute, Utrecht, the Netherlands. [14]Faculty of Electrical Engineering, Mathematics and Computer Science, Delft University of Technology, Delft, the Netherlands.

Corresponding Author: Michiel S. van der Heijden, Department of Medical Oncology, Department of Molecular Carcinogenesis, Netherlands Cancer Institute, Plesmanlaan 121, Amsterdam 1066 CX, the Netherlands. E-mail: ms.vd.heijden@nki.nl

Clin Cancer Res 2025;31:3897–906

doi: 10.1158/1078-0432.CCR-25-0419

Translational Relevance

We studied preoperative ipilimumab and nivolumab in a clinical phase Ib trial (NABUCCO) and found promising response rates. Ipilimumab 3 mg/kg seemed more effective than ipilimumab 1 mg/kg. Nevertheless, approximately half of the patients did not respond. In the current study, we analyzed tumor tissue using various methods for potential biomarkers. A high tumor mutational load, PD-L1 positivity, and low expression of a TGFβ signature were correlated with response. For a response to ipilimumab 1 mg/kg, an inflammatory tumor microenvironment might be important. The $CD8^+TCF7^+$ T-cell density increased in the tumor microenvironment of responders to ipilimumab 3 mg/kg, but not in the nonresponders. Further characterization of two responders by single-cell RNA sequencing revealed that this T-cell subset was enriched with transcripts involved in immunologic memory and T-cell homing. Thus, this multiomic study provides further evidence for response biomarkers in combination immune checkpoint blockade.

rates are encouraging, more than half of the patients do not respond to single-agent ICB.

Patients who do not respond to anti–PD-(L)1 may lack sufficient immune priming by cancer antigens. Insufficient priming and other inhibitory signals could be overcome by inhibiting CTLA-4, resulting in a broader and more intense antitumor immune response (9). Trials in metastatic urothelial cancer, therefore, evaluated the efficacy of the combination of PD-(L)1 and CTLA-4 blockade (10, 11) and demonstrated the antitumor activity of combination ICB.

Recent evidence obtained from a randomized phase III trial of stage III melanoma emphasizes the benefit of ipilimumab (anti–CTLA-4) plus nivolumab (anti–PD-1) as a preoperative treatment strategy (12). In the first NABUCCO cohort, 24 patients with locally advanced urothelial cancer were treated with three cycles of a combination of nivolumab and ipilimumab followed by surgery, which resulted in a pathologic complete response (pCR, ypT0N0) rate of 46%. However, substantial immune-related toxicity (55% grade ≥ 3) was observed (13). To identify the most optimal balance between efficacy and toxicity, we evaluated two dosing regimens of ipilimumab plus nivolumab in cohort 2 of the NABUCCO trial (14). In line with results in metastatic urothelial cancer (11), ipilimumab at a dose of 3 mg/kg seemed more effective as preoperative treatment compared with ipilimumab at a dose of 1 mg/kg (pCR 43% vs. 7%; ref. 14). Despite the encouraging efficacy of preoperative ipilimumab plus nivolumab, almost half of the patients do not respond to this treatment strategy but are still at risk of experiencing adverse events. Better selection criteria are, therefore, needed to identify patients who are unlikely to respond to combination ICB. Several potential biomarkers for ICB response have been studied in urothelial cancer.

PD-L1 has been investigated extensively as a predictor of ICB response. In metastatic urothelial cancer, tumors with high baseline PD-L1 expression had a better clinical outcome following treatment with anti–PD-(L)1 plus anti–CTLA-4 (10, 11). However, in the preoperative setting, the association between PD-L1 positivity and response to combination ICB was inconsistent (13, 15) and displayed conflicting evidence for PD-L1 as a potential biomarker. Tumor foreignness, as reflected by tumor mutational burden (TMB), has been suggested to be associated with response to ICB in various urothelial cancer stages (4, 7, 16–19). Expression of a TGFβ signature has previously been described to correlate with a lack of response to ICB (8, 16). Based on data suggesting a correlation between tertiary lymphoid structures (TLS) and response to ICB (20, 21), we previously explored whether the presence of TLS at baseline could predict response to ipilimumab and nivolumab in the first NABUCCO cohort (13). We observed no correlation between TLS-enriched tumors at baseline and ICB response, but we identified TLS induction upon treatment in responders to ICB (13).

In the current analysis of the full NABUCCO trial population (cohorts 1 and 2), we explored both potential biomarkers for response to combination ICB and treatment dynamics, aiming for a better understanding of the effects of ICB on the urothelial cancer tumor microenvironment (TME).

Patients and Methods

Study design and population

The NABUCCO trial (NCT03387761) is an investigator-initiated prospective phase Ib clinical trial, which was executed in two stages (Supplementary Fig. S1). The first cohort was a single-arm study at the Netherlands Cancer Institute (NKI), in which 24 patients with stage III urothelial cancer (cT3-4aN0M0 or cT1-4aN1-3M0) were treated with ipilimumab 3 mg/kg on day 1, ipilimumab 3 mg/kg plus nivolumab 1 mg/kg on day 22, and nivolumab 3 mg/kg on day 43, followed by resection within 12 weeks after study drug initiation.

In cohort 2, 30 additional patients with stage III urothelial cancer were randomized to either a preoperative ipilimumab-high dosing regimen (arm 2A; ipilimumab 3 mg/kg plus nivolumab 1 mg/kg on day 1, ipilimumab 3 mg/kg plus nivolumab 1 mg/kg on day 22, and nivolumab 3 mg/kg on day 43) or to an ipilimumab-low schedule (arm 2B; ipilimumab 1 mg/kg plus nivolumab 3 mg/kg on day 1, ipilimumab 1 mg/kg plus nivolumab 3 mg/kg on day 22, and nivolumab 3 mg/kg on day 43) followed by resection. Neither the treating physician nor the patients were blinded to the study treatment. Patients in cohort 2 were recruited at the NKI, the University Medical Center Utrecht, and the Radboud University Medical Center Nijmegen, the Netherlands. The full inclusion and exclusion criteria were reported elsewhere (13). The NABUCCO study was approved by the ethical committee of the NKI; all patients signed informed consent before any study procedures. This study was conducted in accordance with the Declaration of Helsinki.

Baseline formalin-fixed, paraffin-embedded (FFPE) tumor tissue and blood were available for all patients before study treatment initiation and were used for further biomarker analysis. Baseline tumor tissue was compared with on-treatment resected tumor tissue (at cystectomy) to study treatment dynamics [CD8PD-1 IHC $n = 40$ baseline vs. $n = 36$ on-treatment; RNA sequencing (RNA-seq) $n = 53$ baseline vs. $n = 39$ on-treatment; multiplex immunofluorescence (mIF) $n = 51$ baseline vs. $n = 42$ on-treatment; Supplementary Fig. S2]. As cohorts 1 and 2A used high ipilimumab dosages, we refer to these arms as ipilimumab-high and consider cohort 2B the ipilimumab-low cohort. For biomarker purposes, we considered patients staged as ≤ypT1N0 at cystectomy as responders.

PD-L1 IHC

PD-L1 IHC (RRID:AB_2833074) on baseline tumor tissue was performed as described previously (22). An experienced uro-

pathologist (M.L. van Montfoort) manually scored baseline PD-L1 positivity in Slidescore (www.slidescore.com). PD-L1 positivity was determined using three different scoring methods: combined positivity score [CPS; number of PD-L1$^+$ cells (tumor + immune cells) over the number of viable tumor cells × 100%; positive if CPS ≥ 10%], tumor proportion score (TPS; number of PD-L1$^+$ tumor cells over the number of viable tumor cells × 100%; positive when TPS ≥1%), and immune cell score (IC; number of PD-L1$^+$ immune cells over the number of viable tumor cells × 100%; positive when IC ≥ 1%). If PD-L1 positivity was unclear, a second pathologist assessed the sample. Disagreement led to exclusion from the analysis. A Fisher's exact test was used to study the association between PD-L1 positivity (categorical variable) at baseline and response to ICB (categorical variable; IBM SPSS Statistics).

CD8/PD-1 IHC

Both baseline and on-treatment FFPE tumor tissue were double-stained with PD-1 (RRID:AB_3073606) and CD8 (RRID:AB_2075537). PD-1 was detected in the first sequence using clone CAL20 (1:250, 60 minutes at 37°C). The PD-1–bound antibody was visualized using anti-mouse NP (RRID:AB_2375277; 12 minutes at 37°C), followed by anti-NP AP (RRID:AB_10756913; 12 minutes at 37°C) and the DISCOVERY Yellow detection kit. In the following sequence, CD8 was detected using clone C8/144B (RRID:AB_3285728; 1:200, 32 minutes at 37°C). CD8 was visualized using anti-mouse HQ for 12 minutes at 37°C, followed by anti-HQ HRP (RRID:AB_3068525; 12 minutes at 37°C) and the DISCOVERY Purple detection kit. Slides were counterstained with hematoxylin and bluing reagent. Materials used for this analysis were from Ventana Medical Systems. Stained slides were uploaded to the HALO software v3.1. For image analysis, the tumor area was annotated manually with a border of 150 μm to include the stromal region, which forms the TME. Due to the absence of cancer cells in the tissue obtained during cystectomy in patients who achieved a pCR, we annotated the fibrotic tissue and immune infiltrate—if present—as this area was most probably the tumor bed. If we could not identify the tumor bed based on fibrosis with immune infiltration, we excluded the sample from further analysis. An Indica Labs Multiplex IHC v3.4.9 analysis algorithm was used for image analysis. The density of CD8$^+$PD1$^+$ cells (cells/mm^2) and the ratio of CD8$^+$PD1$^+$ over the total number of CD8$^+$ cells in the annotated area were determined. Object data were exported for further downstream analysis (R v3.6).

mIF

mIF was performed using antibodies against CD8 (RRID:AB_2075537), CD103 (RRID:AB_11142856), PanCK (RRID:AB_777047), and the TCF7 protein (RRID:AB_2199302). Additional details are described in Supplementary Table S1. Image analysis was performed using the HALO software (v3.5.3577.285, Indica Labs). Based on the annotation of the tumor area on hematoxylin and eosin in Slidescore, as defined by an experienced uro-pathologist (M.L. van Montfoort), the tumor area with a margin of 150 μm was annotated manually on the corresponding multiplexed slide in HALO. If the tumor was in complete regression, we annotated the area with fibrosis and immune infiltration (if present) as the tumor bed. The Indica Labs Highplex FL v4.0.2 analysis algorithm, utilizing artificial intelligence–based nuclei segmentation, was employed for the analysis. Regions of interest were analyzed, and infiltration analysis was conducted using the spatial analysis option in HALO. Cell object data, including each cell's marker expression and x- and y-coordinates, were extracted for phenotype quantification and further downstream analysis using R v3.6. Thresholds for marker positivity were set to the median of 10 expert-optimized slides from the same batch, and those thresholds were applied to all remaining slides to obtain cell-positive classification for each marker. Subsequent analyses were performed on those classifications. Additionally, cell densities (cells/mm^2) were determined by dividing the number of cells by the corresponding tissue area for specific cell phenotypes: CD8$^+$TCF7$^-$CD103$^-$, CD8$^+$TCF7$^+$CD103$^-$, CD8$^+$TCF7$^-$CD103$^+$, and CD8$^+$TCF7$^+$CD103$^+$. To quantify all CD8$^+$ cells, we aggregated phenotypes: CD8$^+$TCF7$^\pm$CD103$^\pm$. In cases where cells exhibited mutually exclusive marker combinations (e.g., panCK$^+$CD8$^+$), they were reclassified based on the marker with the highest relative intensity level.

DNA sequencing and RNA-seq

DNA and RNA were isolated from FFPE tissue. Details about DNA and RNA isolation and sequencing are depicted in Supplementary Table S1. The DNA sequencing reads were aligned to the human genome version 38 using Burrows-Wheeler Aligner 37. Duplicated reads were identified using MarkDuplicates (http://broadinstitute.github.io/picard), and the quality scores were subsequently recalibrated with GATK BaseRecalibrator 4.2.5.0 (RRID:SCR_001876). Somatic single-nucleotide variants and short insertions and deletions were called in tumor samples matched with germline samples using Strelka 2.9.2 (RRID:SCR_005109; ref. 23). Variants were retained if they had a high-reliability score and an allele frequency above 5%. The selected variants were annotated using SnpEff v4.3t (built 2017-11-24). For TMB, we considered all but synonymous, intronic, and intergenic mutations. For biomarker discovery, we used variants categorized as insertions and deletions, missense, frameshift, stop codon gain or loss, splice acceptor or donor, transcriptional disruption, exon loss, and structural interaction variants for downstream analysis. We explored somatic variants in DNA damage response (DDR) genes with clinical significance (24). For this, we excluded variants labeled as (likely) benign in terms of clinical significance, variants previously identified as population or germline SNPs (with TOPMed and CAF annotations showing an alternate allele frequency >5%), and variants predicted as tolerated based on the SIFT score. In DDR variants, we explored alterations in DNA mismatch repair machinery (*MLH1*, *MSH2*, *MSH6*, *PMS1*, and *PMS2*), nucleotide excision repair (*ERCC2-4* and *ERCC5*), homologous recombination (*BRCA1*, *MRE11A*, *NBN*, *RAD50-51*, *RAD51B*, *RAD51D*, *RAD52*, and *RAD54L*), Fanconi anemia (*BRCA2*, *BRIP1*, *FANCA*, *FANCC*, *PALB2*, *RAD51C*, and *BLM*), checkpoint (*ATM*, *ATR*, *CHEK1-2*, and *MDC1*), and others (*POLE*, *MUTYH*, *PARP1*, and *RECQL4*; ref. 25). Copy numbers were called using CNVkit v0.9.6 (26) with copy number ratios (cnr) calculated relative to a pooled normal reference. As we sequenced the data in two batches, a specific pooled normal reference was estimated for each batch. Gene-level cnr were determined as the weighted average cnr for each gene. Deep deletions were defined as $\log_2(\text{cnr}) < -0.7$, shallow deletions as $-0.7 \leq \log_2(\text{cnr}) < -0.5$, and amplifications as $\log_2(\text{cnr}) > 1$. Genomic data were analyzed using the R packages VariantAnnotation v1.24.5 and ComplexHeatmap v1.17.1.

RNA transcript quantification was performed using Salmon v1.1.0 in quantification mode against the gencode_v29_idx reference, applying fragment GC bias correction and validateMappings mode. For single-end RNA-seq data (batch 1), the library type was specified as "A," whereas for paired-end data (batch 2), the library type was set to "ISF." Salmon quantification files were processed with tximport 1.14.2, and transcript annotation was carried out

using AnnotationDbi 1.48.0, biomaRt 2.42.1, and GenomicFeatures 1.38.2. Transcript counts were subsequently mapped and aggregated into gene-level counts. All analysis pipelines were executed using R 3.6.3. We conducted an exploratory data analysis to assess potential batch effects by projecting the data from three batches onto a principal component analysis space. The analysis revealed a significant batch effect between samples sequenced on the HiSeq 2500 system (RRID:SCR_016383; single-end) and those sequenced on the NovaSeq 6000 system (RRID:SCR_016387; paired-end). To account for these experimental differences, we applied the ComBat-Seq batch effect adjustment tool (27) within the sva package 3.50 at the gene count level. This adjustment resulted in a batch-corrected gene count matrix suitable for differential expression analysis. No additional covariate matrix was required for batch adjustment, as both sequencing batches had a similar distribution of sample types. Notably, no batch effect was detected between the two series of samples sequenced on the NovaSeq 6000 system. The batch-corrected gene count matrix was refined by removing genes with zero counts in >80% of samples and excluding genes not annotated by the HUGO Gene Nomenclature Committee. Only genes with a count per million >1 were retained in at least four samples. For duplicated HUGO Gene Nomenclature Committee genes, the mean gene count was computed. The edgeR package v3.28.1 (RRID:SCR_012802) was used to calculate normalization factors to adjust for raw library sizes. Differential expression analysis was performed on the batch-corrected gene count matrix using the DESeq2 package v1.26.0 (RRID:SCR_000154) without log fold change shrinkage, following the standard analysis pipeline. Gene set enrichment analysis was conducted using the fgsea package (v1.12), parsing the list of genes ranked by $\log_2$ fold change with 10,000 permutations, a false discovery rate (FDR) threshold of 5%, and gene set sizes ranging from 15 to 500, focusing on the Hallmark gene sets. To score gene signatures associated with various biological processes, we conducted a thorough literature review and curated gene signatures from various sources, ensuring minimal redundancy among the selected signatures (Supplementary Table S2). To calculate gene signature scores, we normalized the gene counts using counts per million and library sizes, and the average normalized expression of the signature was computed. The signature scores were analyzed on a logarithmic scale, and differences between groups were assessed using a two-sided *t* test (with an unadjusted *P* value threshold of <0.05). We used the consensus classification (28) and The Cancer Genome Atlas classification (29) to classify molecular subtypes. We used Fisher's exact test to ascertain an association between molecular subtypes and ICB response.

Multiomics analysis

We developed a predictive logistic regression multiomics model using features significantly associated with the ICB response at baseline, which were TMB derived from DNA sequencing, TGFβ derived from RNA-seq, and PD-L1 TPS derived from IHC. We estimated the model on all samples and reported the model statistics. To evaluate predictive performance, we reestimated the model, leaving out one patient sample and predicting that sample. As a summary statistic, we used the ROC curve. We showed the correlation between biomarkers using the Pearson correlation. The model comparison was performed using a log-likelihood test.

scRNA-seq

We used fresh bladder tumor tissue obtained during cystectomy from two patients with a pCR to high-dose ipilimumab to perform single-cell RNA-seq (scRNA-seq) of $CD3^+$ cells, as described in Supplementary Table S1. The count matrix provided by our internal Genome Core Facility was converted into a Seurat object using the Seurat package v5.1.0. As quality control steps, we removed cells with no or conflicting hashtags, >25% of their reads aligned to mitochondrial genes, or cells with a very high or low amount of total genes or read counts (*z*-score of log-transformed total gene or read count >2 or ≤2), as these are most likely nonviable or duplicate cells (https://satijalab.org/seurat/articles/pbmc3k_tutorial.html). Additionally, we removed $CD3^+$ cells in which a T-cell receptor RNA was not detected, and we corrected the expression for the following confounders using the ScaleData function of the Seurat package and the harmony package v1.2.1: cell-cycle scores, ribosomal percentages, mitochondrial content (30), total RNA counts, and sample differences. The number of detected genes (features) and total RNAs (counts) per cell were scaled by a factor of 10,000, $\log_{10}$-transformed, and *z*-scored. Cells with counts or features with *z*-scores less than −2 or greater than +2 were removed. $CD8A^+$ cells were filtered based on normalized and scaled gene counts (*CD8A* RNA > −0.5 and *CD4.1* RNA <0). $TCF7^+$ cells were selected based on ≥1 raw *TCF7* gene counts. Differentially expressed genes between $CD8A^+TCF7^+$ and $CD8A^+TCF7^-$ cells were calculated based on the following thresholds: average $\log_2$ fold change >1.5 or < −1.5 and Bonferroni adjusted *P* value > 1×10^{-10}. The $\log_2$ fold change is based on the normalized expression of genes in $CD8A^+TCF7^+$ and $CD8A^+TCF7^-$ cells and is calculated using the FindMarkers function from the Seurat package.

Data availability

The DNA sequencing and RNA-seq data are deposited in the European Genome-phenome Archive under the accession number EGAC00001001648. PD-L1 and response data are available in Supplementary Table S3. Academic (noncommercial) requests for data use will need to be directed to the corresponding author (M.S. van der Heijden) and will be reviewed by the Institutional Review Board of the NKI. Following approval, a data access agreement with the NKI should be signed. All other data are available upon reasonable academic request under similar conditions.

The underlying codes for our main results are available in a GitHub repository: https://github.com/tropicalberto/nabucco_biomarker_manuscript.git.

Results

Baseline biomarkers for response

From February 2018 to April 2021, 54 patients were enrolled in the NABUCCO trial. The representativeness of study participants about sex, age, race, and geography is depicted in Supplementary Table S4. To identify candidate biomarkers associated with treatment response, IHC and whole-exome tumor/germline DNA sequencing and RNA-seq were performed on pretreatment tumor tissue of the full cohort to explore potential differences between responders and nonresponders (Supplementary Fig. S2). We observed a higher TMB in patients who responded to combination ICB compared with nonresponders (**Fig. 1A**; $P = 0.00068$). Previously, mutations in DDR genes were reported to correlate with response to checkpoint inhibition (24). Similarly, we observed alterations in DDR genes more frequently in responders compared with nonresponders (Supplementary Fig. S3; $P = 0.0188$). Data in advanced urothelial cancer and the adjuvant setting indicated that PD-L1 positivity is associated with response to ICB (10, 11, 31),

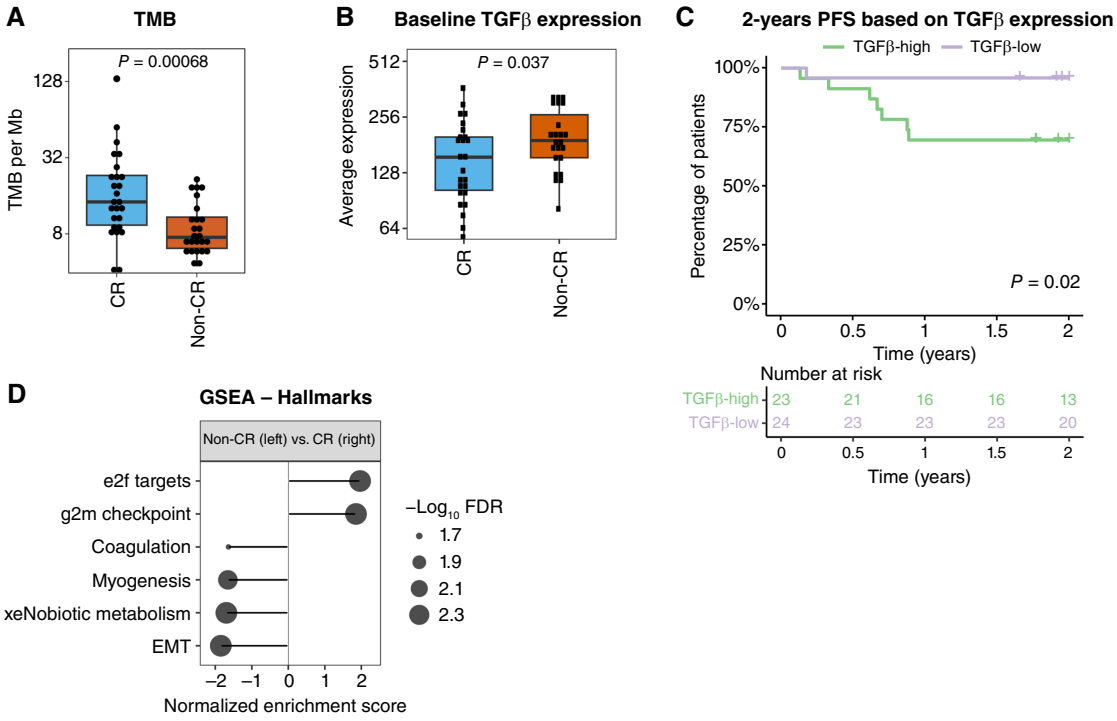

Figure 1.

Baseline biomarkers for response for the full cohort. **A,** Baseline TMB (somatic nonsynonymous TMB per Mb) for responders [complete response (CR); ≤ypT1N0] vs. nonresponders (non-CR; ypT2-4aNx or ypTxN1-3). **B,** Average expression of TGFβ signature (16) between responders and nonresponders. **C,** Progression-free survival for TGFβ-high vs. TGFβ-low (median as cutoff value). The *P* value was calculated using a log-rank test. Clinical cutoff date, March 2022. **D,** Gene set enrichment analysis (GSEA) of baseline hallmark signatures for responders vs. nonresponders; false discovery rate, 5%. EMT, epithelial-to-mesenchymal transition; PFS, progression-free survival.

although conflicting results have been observed (32, 33). In our data, we observed a response to preoperative ipilimumab plus nivolumab more frequently in PD-L1–positive tumors irrespective of the PD-L1 scoring method (**Table 1**; CPS $P = 0.048$; TPS $P = 0.004$; IC $P = 0.016$). Several stromal genes, including those involved in epithelial-to-mesenchymal transition and *TGFβ*, have an immunosuppressive capacity, which could attenuate ICB efficacy (16, 34). We observed that nonresponders showed a higher expression of a fibroblast-derived TGFβ signature (**Fig. 1B**; $P = 0.037$; ref. 16). In addition to a lower pathologic response rate after treatment with ipilimumab plus nivolumab, patients with a high expression of this TGFβ signature showed inferior progression-free survival compared with patients with a low TGFβ expression signature (**Fig. 1C**; $P = 0.02$). Furthermore, patients who were unresponsive to preoperative ipilimumab plus nivolumab showed enhanced expression of an epithelial-to-mesenchymal transition hallmark signature (**Fig. 1D**).

Based on transcriptomic profiling, urothelial tumors can be divided into various molecular subtypes, which we determined for the baseline tumor samples (28, 29). We did not observe a correlation between molecular subtypes and response to ICB (consensus $P = 0.653$; The Cancer Genome Atlas $P = 0.446$; Supplementary Fig. S4). We additionally explored the expression of a TLS signature (20) based on our bulk RNA-seq data and compared responders with nonresponders. We did not observe a difference in TLS-related gene expression across response groups ($P = 0.11$; Supplementary Fig. S5), which is consistent with our previous analysis using mIF in cohort 1 of NABUCCO (13).

To test the predictive potential of our multiomic biomarkers, we constructed a logistic regression model for ICB response with TMB, TGFβ, and PD-L1 TPS as features. We observed that only PD-L1 TPS was robustly associated with ICB response ($P = 0.007$; Supplementary Fig. S6A). The leave-one-out prediction yielded a ROC of 0.789, indicating that TMB, TGFβ, and PD-L1 TPS can predict ICB response (Supplementary Fig. S6B). We found TMB and TGFβ to be negatively correlated (Supplementary Fig. S6C). However, a log-likelihood ratio test revealed that a model without these two terms was significantly worse ($P = 0.0046$), indicating that TMB, TGFβ, and PD-L1 TPS together best predict response. In conclusion, these data indicate that tumors with a high mutational load and PD-L1 positivity at baseline respond better to ipilimumab plus nivolumab, which aligns with data from the PURE-01 study (7). High expression of a TGFβ signature is associated with nonresponse and poor progression-free survival.

Baseline biomarkers for response for ipilimumab-high and ipilimumab-low

From the 54 patients enrolled in the NABUCCO trial, 39 patients were treated with ipilimumab-high (3 mg/kg), and 15 patients received treatment with ipilimumab-low (1 mg/kg). Baseline characteristics were comparable for patients treated with ipilimumab-high

Table 1. Response by PD-L1 CPS, TPS, and IC.

	Responders (≤ypT1N0)	Nonresponders (ypT2-4aNx or ypTxN1-3)	*P* value[a]
CPS			
<10%	7/21 (33%)	14/21 (67%)	0.048
≥10%	19/30 (63%)	11/30 (37%)	
TPS			
<1%	6/23 (26%)	17/23 (74%)	0.004
≥1%	18/26 (72%)	8/26 (31%)	
IC			
<1%	0/7 (0%)	7/7 (100%)	0.016
1%–5%	10/16 (63%)	6/16 (37%)	
≥6%	14/26 (54%)	12/26 (46%)	

[a]*P* values were calculated using a two-sided Fisher's exact test.

and ipilimumab-low and were described previously (14). We explored whether the mutational burden differences between response groups observed for the full cohort were similar for patients treated with ipilimumab-high and ipilimumab-low. We observed that responders had a higher TMB than nonresponders in both the ipilimumab-high and ipilimumab-low groups, but this difference was only significant for ipilimumab-high, most likely due to a lack of statistical power in the ipilimumab-low group ($P = 0.0051$ and $P = 0.24$; Supplementary Fig. S7). Next, we evaluated potential transcriptomic differences in response groups for both ipilimumab dosing regimens. Responders to ipilimumab-high showed enhanced transcription of hallmarks for the g2m checkpoint and e2f targets (**Fig. 2A** and **B**). We identified that responders to ipilimumab-low showed enrichment of IFN-α and IFN-γ hallmarks and an increased expression of inhibitory immune checkpoints, including *PD-L1* and *CTLA-4*, indicating a more inflammatory TME (**Fig. 2C** and **D**). Next, we studied the TME for $CD8^+$ T-cell infiltration in both ipilimumab dosing regimens and compared responders with nonresponders. In the ipilimumab-high group, the density of various $CD8^+$ T-cell subsets was similar for responders compared with nonresponders (Supplementary Fig. S8A). In the ipilimumab-low cohort, densities of unselected $CD8^+$ T cells, $CD8^+CD103^+$ T cells (tissue-resident T cells), and $CD8^+$-$PD1^+$ T cells were numerically higher in responders compared with nonresponders, but statistical significance was not reached (Supplementary Fig. S8B). Results from this exploratory analysis suggest that a TME with inflammatory characteristics at baseline might be required for a response to low-dose ipilimumab, whereas a response to high-dose ipilimumab seemed less dependent on an inflamed TME.

Treatment dynamics

To examine the effects of ipilimumab plus nivolumab on the TME, we explored the characteristics of infiltrating $CD8^+$ T cells in baseline and on-treatment samples using a T-cell mIF panel with markers for tissue-resident T cells ($CD103^+$) and stem-like memory T cells ($TCF7^+$). We evaluated the infiltration of $CD8^+CD103^+$ cells in the TME as we assumed that $CD8^+CD103^+$ T cells are tumor-reactive (35). $CD8^+TCF7^+$ T cells have been described to play an important role in ICB efficacy, given their potential to form immunologic memory (36). In the full cohort, both the total $CD8^+$ T-cell density ($P = 0.0018$) and the $CD8^+TCF7^+$ T-cell density ($P = 0.0077$) increased upon combination ICB, whereas the densities of $CD8^+CD103^+$ T cells ($P = 0.14$) and $CD8^+PD1^+$ T cells ($P = 0.14$) were similar in baseline and on-treatment tissue (**Fig. 3A**). However, there was a decline in the ratio of $CD8^+PD1^+$ T cells over the total $CD8^+$ T cells following combination ICB ($P = 0.00016$; **Fig. 3B**), possibly as a direct result of therapy targeting PD-1. To elucidate which changes in the TME characterize a treatment response, we examined treatment dynamics in responders (≤ypT1N0) and nonresponders (ypT2-4aNx or ypTxN1-3) in both dosing regimens. Interestingly, only in responders to ipilimumab-high, both the total $CD8^+$ T-cell density ($P = 0.0029$) and the $CD8^+TCF7^+$ T-cell subset ($P = 0.0015$) accumulated in the TME following treatment (**Fig. 3C**). This phenomenon was not observed in nonresponders to ipilimumab-high (**Fig. 3D**). In the ipilimumab-low cohort, $CD8^+$ T-cell densities were similar in pre- and on-treatment tissue (**Fig. 3E** and **F**); however, this analysis was limited by a low sample size.

The $CD8^+TCF7^+$ T-cell subset was previously described as contributing to an ICB-mediated antitumor response (37). Therefore, we aimed to characterize this particular subset in more detail. We performed scRNA-seq of isolated $CD3^+$ T cells in the on-treatment bladder tissue of two responders to high-dose ipilimumab (both ypT0N0). The change in $CD8^+TCF7^+$ T-cell infiltration at baseline and on-treatment, visualized by mIF, is illustrated for these two samples in Supplementary Fig. S9. The scRNA-seq experiment comprised 11,607 $CD3^+$ cells. After quality control and filtering, we were left with 3,027 $CD3^+$ cells for sample #1 and 868 $CD3^+$ cells for sample #14. In sample #1, 2,372 cells were *CD8A*$^+$, and in sample #14, 429 cells were *CD8A*$^+$. Out of the 2,372 *CD8A*$^+$ cells in sample #1, 156 cells (6.6%) were positive for *TCF7*. In sample #14, 139 cells (32.4%) were *CD8A*$^+$*TCF7*$^+$. The remaining *CD8A*$^+$ T cells were *TCF7*$^-$. The fraction of *CD8A*$^+$*TCF7*$^+$ cells in our scRNA-seq data aligns with our mIF data: 5.6% $CD8^+TCF7^+$ in sample #1 and 33% $CD8^+TCF7^+$ in sample #14. When comparing the RNA expression of *CD8A*$^+$*TCF7*$^+$ cells with *CD8A*$^+$*TCF7*$^-$ cells, we found an enhanced expression of *IL7R* and *SELL* (**Fig. 3G**), which suggests that *CD8A*$^+$*TCF7*$^+$ cells are in transition from an effector to a memory state (38). Furthermore, we observed enhanced transcription of *LEF1* in the *CD8A*$^+$*TCF7*$^+$ subset, a transcription factor that mainly acts during thymocyte maturation. Together with *TCF7*, *LEF1* seems to be involved in memory formation (39). Also, the expression of *GPR15*, *CCR7*, and *XCL1* was found to be upregulated in *CD8A*$^+$*TCF7*$^+$ T cells, suggesting activated migration programs in these cells (40, 41). In summary, combination ICB increased the total $CD8^+$ T-cell density and the $CD8^+TCF7^+$ T-cell density. Our data in responders suggest an increase in the density of $CD8^+TCF7^+$ T cells in the TME following high-dose ipilimumab. The focused analysis of two responders to ipilimumab-high indicated that *CD8A*$^+$*TCF7*$^+$ T cells possess characteristics of memory cells with migratory potential.

Discussion

In the NABUCCO trial, we studied preoperative ipilimumab plus nivolumab in patients with locally advanced urothelial cancer, showing encouraging response rates. Given the increasing availability of effective treatment regimens for urothelial cancer (6, 42), biomarkers are needed to identify patients who are likely to benefit from specific therapies. In this study, we report a comprehensive exploratory biomarker analysis from the full NABUCCO cohort. We found that high TMB at baseline is associated with response to combination ICB, which is in line with previous studies with anti–

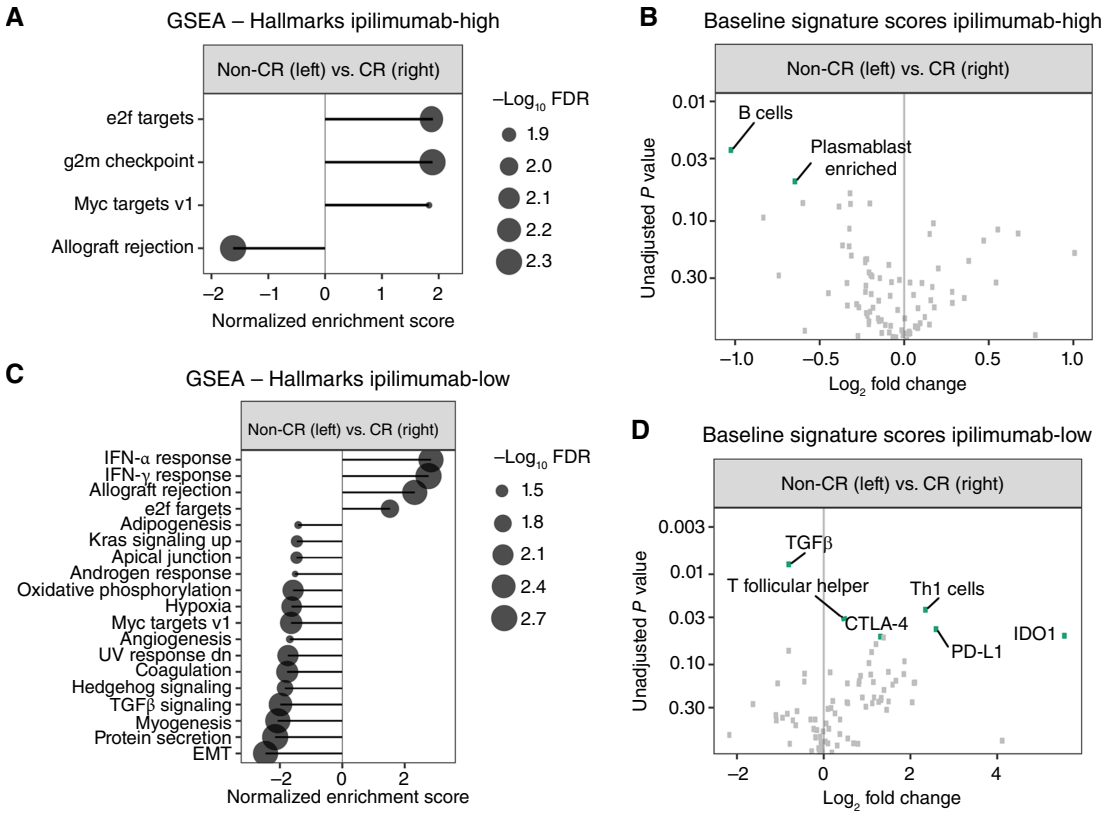

Figure 2.

Transcriptomic differences between responders and nonresponders at baseline for ipilimumab-high and ipilimumab-low. **A,** Gene set enrichment analysis (GSEA) of baseline hallmark signatures for responders (≤ypT1N0) vs. nonresponders (ypT2-4aNx or ypTxN1-3) in ipilimumab-high (arms 1 + 2A); false discovery rate (FDR), 5%. **B,** Differentially expressed signature scores at baseline for responders vs. nonresponders in ipilimumab-high (arms 1 + 2A). **C,** GSEA of baseline hallmark signatures for responders vs. nonresponders in ipilimumab-low (arm 2B); FDR, 5%. **D,** Differentially expressed signature scores at baseline for responders vs. nonresponders in ipilimumab-low (arm 2B).

PD-(L)1 monotherapy in metastatic urothelial cancer (4, 16–19, 43). In the preoperative setting, similar results about TMB and response to anti–PD-1 were observed in the PURE-01 study (7). In contrast, high TMB at baseline did not correlate with response to other preoperative checkpoint inhibitors such as durvalumab (anti–PD-L1) and tremelimumab (anti–CTLA-4; ref. 15).

Furthermore, our data indicate that high expression of TGFβ signature genes at baseline is associated with resistance to ipilimumab plus nivolumab. Our results are in line with a prior study in metastatic urothelial cancer, demonstrating the association between TGFβ and nonresponse (16). Similarly, in another preoperative ICB study in urothelial bladder cancer (ABACUS), increased *FAP* (fibroblast activation protein) expression—which is associated with TGFβ signaling (44)—was associated with resistance to preoperative atezolizumab (8). Although the exact mechanism is not entirely understood, the hypothesis is that TGFβ-induced fibrosis may create a physical barrier that hinders immune cells from reaching cancer cells (8).

In this study, PD-L1 positivity at baseline was significantly associated with response to ipilimumab plus nivolumab, regardless of the scoring method. The predictive value of TPS seemed superior compared with CPS and IC. PD-L1 expression as a predictor of response to checkpoint inhibitors remains controversial in urothelial and other cancers. Results obtained from CheckMate 274, a trial with adjuvant nivolumab in high-risk muscle-invasive bladder cancer (31), showed an enrichment of clinical benefit in patients who were PD-L1–positive by the TPS algorithm. In contrast, the AMBASSADOR trial of adjuvant pembrolizumab in a similar population and trial design did not show a predictive effect when using the CPS algorithm (32). These results could be seen as in line with our finding that TPS may have a higher predictive potential than CPS, although the sample size in our study is insufficient to directly compare scoring algorithms.

A surprising finding in our previous analysis of NABUCCO cohort 1 was the lack of association of preexisting T-cell immunity with response to treatment (13). We hypothesized that anti–CTLA-4 could induce or broaden newly formed anticancer immune responses, leading to inflammation upon treatment initiation (9). Our observation that responders to ipilimumab-low had a TME with inflammatory characteristics before treatment supports the idea that CTLA-4 blockade might augment preexisting immunity and that ipilimumab-low is inferior in achieving this effect, necessitating preexisting T-cell immunity to induce a pCR. Overall, the reduced response rate and correlation with preexisting immunity in the ipilimumab-low cohort seem more in line with the results of anti–PD-(L)1 monotherapy than with the added

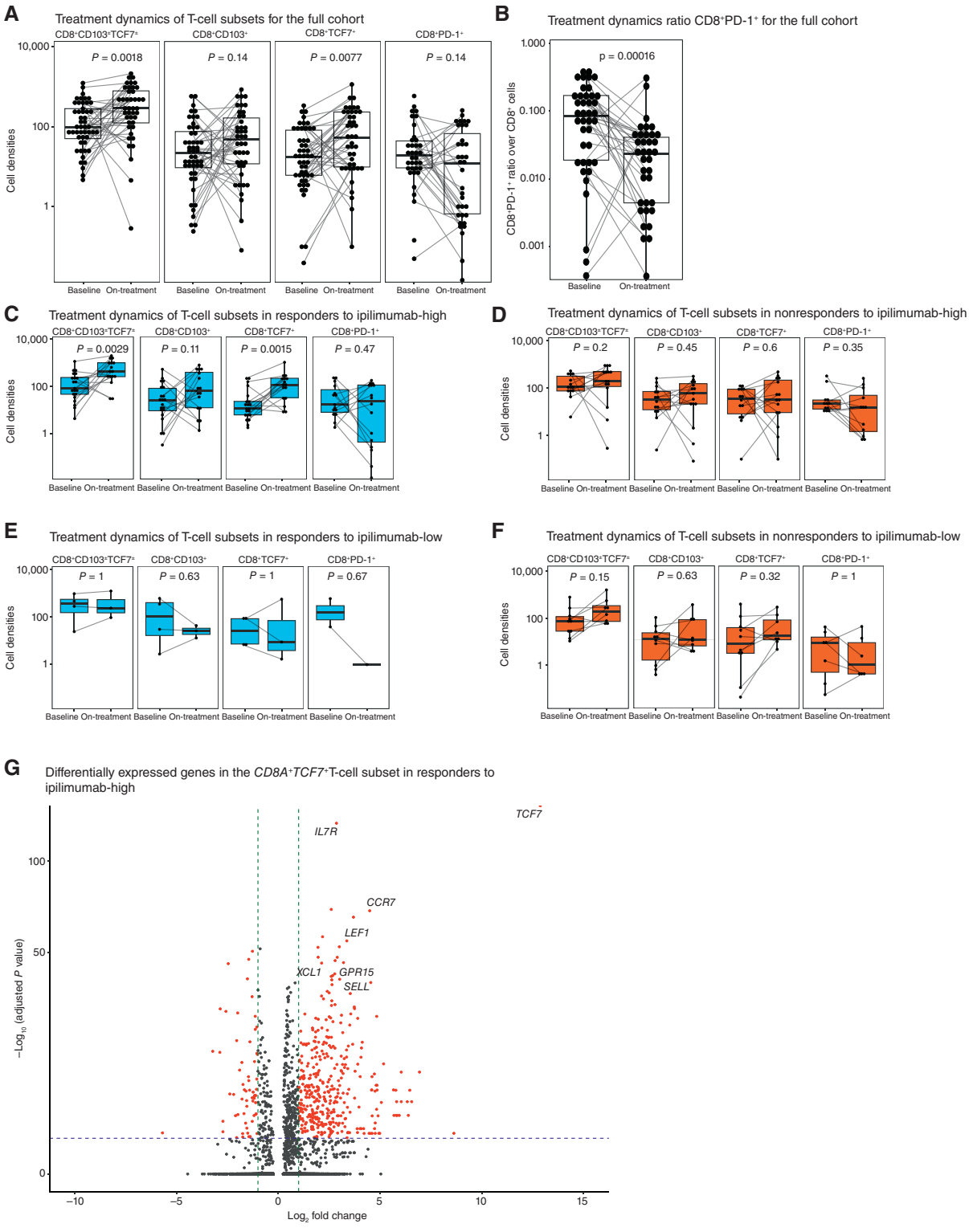

Figure 3.

A, Dynamics in CD8$^+$ T-cell subsets for the full cohort (arms 1 + 2A + 2B). Number of paired samples: CD8$^+$, CD8$^+$CD103$^+$, and CD8$^+$TCF7$^+$ $n = 40$; CD8$^+$PD1$^+$ $n = 32$. **B,** Dynamics in the ratio of CD8$^+$PD1$^+$ over CD8$^+$ cells for the full cohort (arm 1 + 2A + 2B), 32 paired samples. **C,** Dynamics in CD8$^+$ T-cell subsets for responders (≤ypT1N0) following ipilimumab-high (arms 1 + 2A). **D,** Dynamics in CD8$^+$ T-cell subsets for nonresponders (ypT2-4aNx or ypTxN1-3) following ipilimumab-high (arms 1 + 2A). **E,** Dynamics in CD8$^+$ T-cell subsets for responders following ipilimumab-low (arm 2B). **F,** Dynamics in CD8$^+$ T-cell subsets for nonresponders following ipilimumab-low (arm 2B). **G,** Differentially expressed genes in *CD8A*$^+$*TCF7*$^+$ cells vs. *CD8A*$^+$*TCF7*$^-$ cells in responders to ipilimumab-high. Overexpressed genes are depicted on the right.

benefit of ipilimumab-high, suggesting that higher doses of ipilimumab are required to induce an anticancer immune response in urothelial cancers with a "cold" TME. Our sample size in the ipilimumab-low cohort prevents us from drawing definitive conclusions on this hypothesis.

A novel observation in our analysis is the increased density of $CD8^+TCF7^+$ T cells in the TME following combination ICB. Further evaluation of this result showed that the increase in the density of these cells originated from responders to ipilimumab-high, which indicates that ipilimumab-high may be required to achieve an accumulation of this T-cell subset within the TME, and that this subset could be important for an effective antitumor immune response. We did not observe this increase in the ipilimumab-low cohort; however, this cohort had a small sample size, warranting caution in the interpretation of this result. We confirmed the presence of this T-cell subset on treatment in a similar ratio in two responders to ipilimumab-high using scRNA-seq. We further characterized the *CD8A*$^+$*TCF7*$^+$ T cells after treatment and identified enhanced expression of *IL7R*, *SELL*, *LEF1*, *CCR7*, *GPR15*, and *XCL1*, which led to our hypothesis that *CD8A*$^+$*TCF7*$^+$ cells represent a transition away from effector T cells, driving the effective anticancer immune response toward a memory T-cell population (38). This T-cell subset also possesses transcripts required for homing toward secondary lymphoid structures (41).

An important limitation is the absence of scRNA-seq data on baseline tissue, which precludes validation of treatment dynamics observed with mIF. Another limitation of our study, in general, is the small sample size, which limits statistical power, especially in the ipilimumab-low cohort. Additionally, we considered arms 1 and 2A as ipilimumab-high, given the comparable response rates in these arms, but the treatment regimens in these cohorts were not completely identical.

In conclusion, our exploratory biomarker analysis indicates that tumors with a high mutational burden and baseline PD-L1 positivity exhibit a better response to preoperative combination ICB, whereas high expression of a TGFβ signature is linked to nonresponse. A TME with signs of inflammation at baseline may be important for a response to low-dose ipilimumab. An analysis of TME treatment dynamics revealed enrichment of $CD8^+TCF7^+$ T cells. In an exploratory analysis of two responders to high-dose ipilimumab, *CD8A*$^+$*TCF7*$^+$ T cells displayed features indicative of memory formation.

Authors' Disclosures

B.W.G van Rhijn reports other support from Incyte International Biosciences outside the submitted work. L.S. Mertens reports other support from Merck and J&J outside the submitted work. J.M. de Feijter reports grants from Bristol Myers Squibb during the conduct of the study as well as personal fees from Johnson & Johnson outside the submitted work. A.G. van der Heijden reports personal fees from Merck Sharp & Dohme and Merck and grants from Astellas, AstraZeneca, Merck, Johnson & Johnson, and Bristol Myers Squibb outside the submitted work. R.P. Meijer reports grants from Merck B.V., Janssen–Cilag B.V., Astellas Pharma Europe, and Gilead Sciences Netherlands B.V. and other support from Merck B.V. outside the submitted work. W. Scheper reports personal fees from BD Biosciences and Lumicks BV outside the submitted work. L.F.A. Wessels reports grants from Bristol Myers Squibb outside the submitted work. M.S. van der Heijden reports grants, personal fees, and nonfinancial support from Bristol Myers Squibb during the conduct of the study; grants and personal fees from AstraZeneca and MSD; personal fees from Astellas, Daiichi Sankyo, Pfizer/Seagen, and Janssen; and grants from Roche and 4SC outside the submitted work. No disclosures were reported by the other authors.

Authors' Contributions

C.F. Stockem: Conceptualization, resources, data curation, formal analysis, investigation, methodology, writing–original draft, project administration. **A. Gil-Jimenez:** Conceptualization, data curation, software, formal analysis, investigation, methodology, writing–review and editing. **H. Ali:** Software, formal analysis, investigation, methodology, writing–review and editing. **J. van Dorp:** Resources, validation, methodology, project administration, writing–review and editing. **N. van Dijk:** Resources, methodology, project administration, writing–review and editing. **M.L. van Montfoort:** Resources, investigation, writing–review and editing. **M. Alkemade:** Investigation, writing–review and editing. **A. Broeks:** Resources, methodology, writing–review and editing. **I.M. Seignette:** Investigation, methodology, writing–review and editing. **E. Hooijberg:** Methodology, writing–review and editing. **W. Brugman:** Resources, investigation, writing–review and editing. **R. Voogd:** Resources, investigation, writing–review and editing. **B.W.G. van Rhijn:** Resources, methodology, writing–review and editing. **L.S. Mertens:** Resources, writing–review and editing. **J.M. de Feijter:** Resources, writing–review and editing. **N. Mehra:** Resources, writing–review and editing. **A.G. van der Heijden:** Resources, writing–review and editing. **R.P. Meijer:** Resources, writing–review and editing. **B.B.M. Suelmann:** Resources, writing–review and editing. **W. Scheper:** Resources, data curation, methodology, writing–review and editing. **L.F.A. Wessels:** Data curation, supervision, methodology, writing–review and editing. **D.J. Vis:** Data curation, software, supervision, methodology, writing–review and editing. **M.S. van der Heijden:** Conceptualization, resources, data curation, supervision, funding acquisition, investigation, methodology, project administration, writing–review and editing.

Acknowledgments

We would like to acknowledge the NKI-AVL Core Facility Molecular Pathology & Biobanking for their lab support and the NKI's Research High-Performance Compute facility for providing computational facilities. We thank BMS for funding and supplying ipilimumab and nivolumab to conduct the NABUCCO study. We would further like to acknowledge the patients participating in the NABUCCO trial and their families, as well as the clinical study teams at the participating centers.

Note

Supplementary data for this article are available at Clinical Cancer Research Online (http://clincancerres.aacrjournals.org/).

Received February 5, 2025; revised April 17, 2025; accepted June 3, 2025; posted first June 9, 2025.

References

1. Pfister C, Gravis G, Flechon A, Chevreau C, Mahammedi H, Laguerre B, et al. Perioperative dose-dense methotrexate, vinblastine, doxorubicin, and cisplatin in muscle-invasive bladder cancer (VESPER): survival endpoints at 5 years in an open-label, randomised, phase 3 study. Lancet Oncol 2024;25:255–64.
2. Bellmunt J, de Wit R, Vaughn DJ, Fradet Y, Lee JL, Fong L, et al. Pembrolizumab as second-line therapy for advanced urothelial carcinoma. N Engl J Med 2017;376:1015–26.
3. Powles T, Eder JP, Fine GD, Braiteh FS, Loriot Y, Cruz C, et al. MPDL3280A (anti-PD-L1) treatment leads to clinical activity in metastatic bladder cancer. Nature 2014;515:558–62.
4. Rosenberg JE, Hoffman-Censits J, Powles T, van der Heijden MS, Balar AV, Necchi A, et al. Atezolizumab in patients with locally advanced and metastatic urothelial carcinoma who have progressed following treatment with platinum-based chemotherapy: a single-arm, multicentre, phase 2 trial. Lancet 2016;387:1909–20.
5. Versluis JM, Long GV, Blank CU. Learning from clinical trials of neoadjuvant checkpoint blockade. Nat Med 2020;26:475–84.
6. Powles T, Catto JWF, Galsky MD, Al-Ahmadie H, Meeks JJ, Nishiyama H, et al. Perioperative durvalumab with neoadjuvant chemotherapy in operable bladder cancer. N Engl J Med 2024;391:1773–86.
7. Necchi A, Anichini A, Raggi D, Briganti A, Massa S, Lucianò R, et al. Pembrolizumab as neoadjuvant therapy before radical cystectomy in patients with

muscle-invasive urothelial bladder carcinoma (PURE-01): an open-label, single-arm, phase II study. J Clin Oncol 2018;36:3353–60.
8. Powles T, Kockx M, Rodriguez-Vida A, Duran I, Crabb SJ, Van Der Heijden MS, et al. Clinical efficacy and biomarker analysis of neoadjuvant atezolizumab in operable urothelial carcinoma in the ABACUS trial. Nat Med 2019;25: 1706–14.
9. Stockem CF, Galsky MD, van der Heijden MS. Turning up the heat: CTLA4 blockade in urothelial cancer. Nat Rev Urol 2024;21:22–34.
10. Powles T, van der Heijden MS, Castellano D, Galsky MD, Loriot Y, Petrylak DP, et al. Durvalumab alone and durvalumab plus tremelimumab versus chemotherapy in previously untreated patients with unresectable, locally advanced or metastatic urothelial carcinoma (DANUBE): a randomised, open-label, multicentre, phase 3 trial. Lancet Oncol 2020;21:1574–88.
11. Sharma P, Siefker-Radtke A, de Braud F, Basso U, Calvo E, Bono P, et al. Nivolumab alone and with ipilimumab in previously treated metastatic urothelial carcinoma: CheckMate 032 nivolumab 1 mg/kg plus ipilimumab 3 mg/kg expansion cohort results. J Clin Oncol 2019;37:1608–16.
12. Blank CU, Lucas MW, Scolyer RA, van de Wiel BA, Menzies AM, Lopez-Yurda M, et al. Neoadjuvant nivolumab and ipilimumab in resectable stage III melanoma. N Engl J Med 2024;391:1696–708.
13. van Dijk N, Gil-Jimenez A, Silina K, Hendricksen K, Smit LA, de Feijter JM, et al. Preoperative ipilimumab plus nivolumab in locoregionally advanced urothelial cancer: the NABUCCO trial. Nat Med 2020;26:1839–44.
14. van Dorp J, Pipinikas C, Suelmann BBM, Mehra N, van Dijk N, Marsico G, et al. High- or low-dose preoperative ipilimumab plus nivolumab in stage III urothelial cancer: the phase 1B NABUCCO trial. Nat Med 2023;29:588–92.
15. Gao J, Navai N, Alhalabi O, Siefker-Radtke A, Campbell MT, Tidwell RS, et al. Neoadjuvant PD-L1 plus CTLA-4 blockade in patients with cisplatin-ineligible operable high-risk urothelial carcinoma. Nat Med 2020;26:1845–51.
16. Mariathasan S, Turley SJ, Nickles D, Castiglioni A, Yuen K, Wang Y, et al. TGFβ attenuates tumour response to PD-L1 blockade by contributing to exclusion of T cells. Nature 2018;554:544–8.
17. Snyder A, Nathanson T, Funt SA, Ahuja A, Buros Novik J, Hellmann MD, et al. Contribution of systemic and somatic factors to clinical response and resistance to PD-L1 blockade in urothelial cancer: an exploratory multi-omic analysis. PLoS Med 2017;14:e1002309.
18. Miao D, Margolis CA, Vokes NI, Liu D, Taylor-Weiner A, Wankowicz SM, et al. Genomic correlates of response to immune checkpoint blockade in microsatellite-stable solid tumors. Nat Genet 2018;50:1271–81.
19. Balar AV, Galsky MD, Rosenberg JE, Powles T, Petrylak DP, Bellmunt J, et al. Atezolizumab as first-line treatment in cisplatin-ineligible patients with locally advanced and metastatic urothelial carcinoma: a single-arm, multicentre, phase 2 trial. Lancet 2017;389:67–76.
20. Cabrita R, Lauss M, Sanna A, Donia M, Skaarup Larsen M, Mitra S, et al. Tertiary lymphoid structures improve immunotherapy and survival in melanoma. Nature 2020;577:561–5.
21. Helmink BA, Reddy SM, Gao J, Zhang S, Basar R, Thakur R, et al. B cells and tertiary lymphoid structures promote immunotherapy response. Nature 2020; 577:549–55.
22. Chelushkin MA, van Dorp J, van Wilpe S, Seignette IM, Mellema JJ, Alkemade M, et al. Platinum-based chemotherapy induces opposing effects on immunotherapy response-related spatial and stromal biomarkers in the bladder cancer microenvironment. Clin Cancer Res 2024;30:4227–39.
23. Kim S, Scheffler K, Halpern AL, Bekritsky MA, Noh E, Källberg M, et al. Strelka2: fast and accurate calling of germline and somatic variants. Nat Methods 2018;15:591–4.
24. Teo MY, Seier K, Ostrovnaya I, Regazzi AM, Kania BE, Moran MM, et al. Alterations in DNA damage response and repair genes as potential marker of clinical benefit from PD-1/PD-L1 blockade in advanced urothelial cancers. J Clin Oncol 2018;36:1685–94.
25. Necchi A, Raggi D, Gallina A, Madison R, Colecchia M, Lucianò R, et al. Updated results of PURE-01 with preliminary activity of neoadjuvant pembrolizumab in patients with muscle-invasive bladder carcinoma with variant histologies. Eur Urol 2020;77:439–46.
26. Talevich E, Shain AH, Botton T, Bastian BC. CNVkit: genome-wide copy number detection and visualization from targeted DNA sequencing. PLoS Comput Biol 2016;12:e1004873.
27. Zhang Y, Parmigiani G, Johnson WE. ComBat-seq: batch effect adjustment for RNA-seq count data. NAR Genom Bioinform 2020;2:lqaa078.
28. Kamoun A, de Reyniès A, Allory Y, Sjödahl G, Robertson AG, Seiler R, et al. A consensus molecular classification of muscle-invasive bladder cancer. Eur Urol 2020;77:420–33.
29. Robertson AG, Kim J, Al-Ahmadie H, Bellmunt J, Guo G, Cherniack AD, et al. Comprehensive molecular characterization of muscle-invasive bladder cancer. Cell 2017;171:540–56.e25.
30. Moravec Z, Zhao Y, Voogd R, Cook DR, Kinrot S, Capra B, et al. Discovery of tumor-reactive T cell receptors by massively parallel library synthesis and screening. Nat Biotechnol 2025;43:214–22.
31. Bajorin DF, Witjes JA, Gschwend JE, Schenker M, Valderrama BP, Tomita Y, et al. Adjuvant nivolumab versus placebo in muscle-invasive urothelial carcinoma. N Engl J Med 2021;384:2102–14.
32. Apolo AB, Ballman KV, Sonpavde G, Berg S, Kim WY, Parikh R, et al. Adjuvant pembrolizumab versus observation in muscle-invasive urothelial carcinoma. N Engl J Med 2025;392:45–55.
33. Powles T, Durán I, van der Heijden MS, Loriot Y, Vogelzang NJ, De Giorgi U, et al. Atezolizumab versus chemotherapy in patients with platinum-treated locally advanced or metastatic urothelial carcinoma (IMvigor211): a multicentre, open-label, phase 3 randomised controlled trial. Lancet 2018; 391:748–57.
34. Wang L, Saci A, Szabo PM, Chasalow SD, Castillo-Martin M, Domingo-Domenech J, et al. EMT- and stroma-related gene expression and resistance to PD-1 blockade in urothelial cancer. Nat Commun 2018;9:3503.
35. Duhen T, Duhen R, Montler R, Moses J, Moudgil T, de Miranda NF, et al. Co-expression of CD39 and CD103 identifies tumor-reactive CD8 T cells in human solid tumors. Nat Commun 2018;9:2724.
36. Sade-Feldman M, Yizhak K, Bjorgaard SL, Ray JP, de Boer CG, Jenkins RW, et al. Defining T cell states associated with response to checkpoint immunotherapy in melanoma. Cell 2018;175:998–1013.e20.
37. Wen S, Lu H, Wang D, Guo J, Dai W, Wang Z. TCF-1 maintains $CD8^+$ T cell stemness in tumor microenvironment. J Leukoc Biol 2021;110:585–90.
38. Kaech SM, Tan JT, Wherry EJ, Konieczny BT, Surh CD, Ahmed R. Selective expression of the interleukin 7 receptor identifies effector CD8 T cells that give rise to long-lived memory cells. Nat Immunol 2003;4:1191–8.
39. Zhou X, Xue HH. Cutting edge: generation of memory precursors and functional memory CD8+ T cells depends on T cell factor-1 and lymphoid enhancer-binding factor-1. J Immunol 2012;189:2722–6.
40. Okamoto Y, Shikano S. Emerging roles of a chemoattractant receptor GPR15 and ligands in pathophysiology. Front Immunol 2023;14:1179456.
41. Kobayashi D, Endo M, Ochi H, Hojo H, Miyasaka M, Hayasaka H. Regulation of CCR7-dependent cell migration through CCR7 homodimer formation. Sci Rep 2017;7:8536.
42. Powles T, Valderrama BP, Gupta S, Bedke J, Kikuchi E, Hoffman-Censits J, et al. Enfortumab vedotin and pembrolizumab in untreated advanced urothelial cancer. N Engl J Med 2024;390:875–88.
43. Boll LM, Vázquez Montes de Oca S, Camarena ME, Castelo R, Bellmunt J, Perera-Bel J, et al. Predicting immunotherapy response of advanced bladder cancer through a meta-analysis of six independent cohorts. Nat Commun 2025;16:1213.
44. Wynn TA, Ramalingam TR. Mechanisms of fibrosis: therapeutic translation for fibrotic disease. Nat Med 2012;18:1028–40.